

PAPER • OPEN ACCESS

## Research on Corrosion Characteristics of Towers and Grounding Grids in Power Systems

To cite this article: Xiaopo Mao *et al* 2023 *J. Phys.: Conf. Ser.* **2662** 012020

View the [article online](#) for updates and enhancements.

You may also like

- [Corrosion fault identification model of substation grounding grid based on PSO-LS-SVM](#)

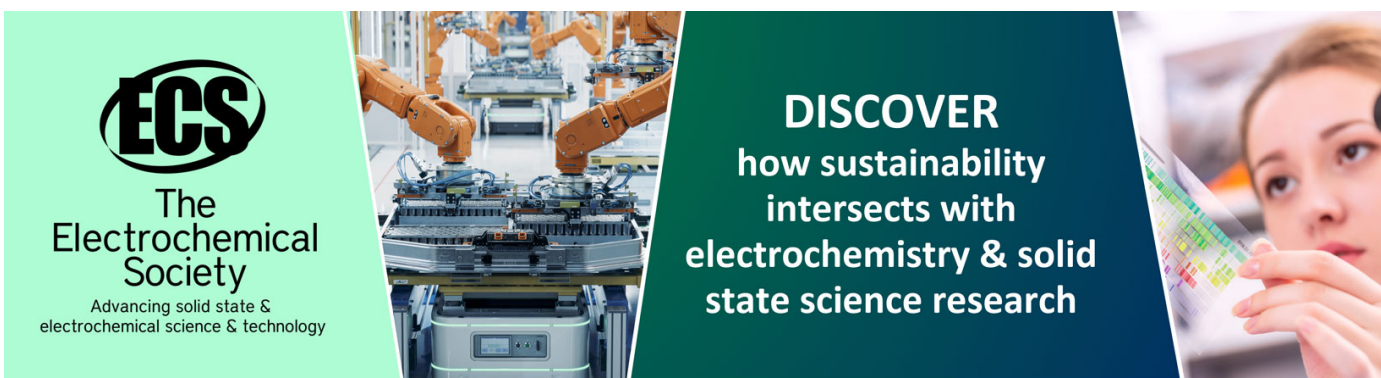
Jun Qin, Jin Miao, Xi Wu *et al.*

- [Study on Corrosion Characteristics of Grounding Materials in High Corrosion Area](#)

Mingxiang Huang and Jianxun Zhang

- [Experimental Investigation of Surge Propagation Characteristics on a Substation Grounding System](#)

V V Kolobov, M B Barannik and V V Ivonin



**ECS**  
The  
Electrochemical  
Society  
Advancing solid state &  
electrochemical science & technology

**DISCOVER**  
how sustainability  
intersects with  
electrochemistry & solid  
state science research

# Research on Corrosion Characteristics of Towers and Grounding Grids in Power Systems

Xiaopo Mao<sup>1\*</sup>, Qiuju Cui<sup>2</sup>, Jianfeng Ye<sup>1</sup>, Xin Li<sup>2</sup>, Liang Gao<sup>1</sup>, Haibo Yang<sup>1</sup>, Weiming Yan<sup>3</sup>, Ze Tian<sup>1</sup>, Yu Xiong<sup>3</sup>

<sup>1</sup> Electric Power Research Institute, State Grid Hubei Electric Power Corporation, Wuhan 430077, China

<sup>2</sup> State Grid Hubei Electric Power Corporation, Wuhan 430077, China

<sup>3</sup> Hubei Fangyuan Dongli Electric Power Science Research Co., Ltd., Wuhan 430077, China

\* Corresponding author's e-mail: mxp2004@163.com

**Abstract:** Due to the increasingly severe corrosion of transmission line towers and grounding grids by the environment in which they are located, we analyse the corrosion characteristics of transmission line towers and grounding grids and provide a theoretical basis for the stable operation of the power grid. This article studies the corrosion components composed of various factors, including water content, temperature, potential difference, area ratio of the cathode to anode, and accelerated corrosion time, through experimental simulation of heavy industrial pollution environment. The research results indicate that water content, potential difference between positive and negative electrodes, area ratio of positive and negative electrodes, and test temperature significantly impact the accelerated corrosion rate test results.

## 1. Introduction

Falk et al. conducted atmospheric exposure and accelerated tests on carbon steel, introducing SO<sub>2</sub> and maintaining the same deposition rate in both tests, and found good consistency between the two<sup>[1]</sup>. Jin Lei et al. used nine types of accelerated tests and analyzed the results curves of carbon steel accelerated tests and outdoor exposure tests<sup>[2]</sup>. It is believed that there is a certain correlation between the accelerated tests and outdoor exposure tests. Lyon et al. believed that using the dry, wet, alternating method in accelerated testing correlates better with salt spray testing<sup>[3]</sup>. Focusing on humidity and condensation can accelerate testing results closer to natural exposure. Drazic et al. used two acceleration methods for low alloy Cr Mo steel: cyclic immersion (3% NaCl) and salt spray test, which showed that the long-term atmospheric corrosion behavior of the material can be predicted based on the analysis of short-term acceleration test results<sup>[4-5]</sup>.

Industrial development has improved material levels, while much environmental pollution has emerged. Industrial waste gas has become the largest factor in atmospheric pollutants, and the continuous flow of air has caused an increasing impact on the operating environment of the power grid, accelerating the rate of corrosion<sup>[6-7]</sup>.

Due to the environmental pollution caused by industry, it is influenced by natural and human factors and has complex and ever-changing characteristics<sup>[8-10]</sup>. This article uses accelerated corrosion technology to simulate the corrosion development of towers and grounding grids in heavy industrial pollution environments, including temperature and humidity fluctuations, salt spray, ultraviolet



radiation, and various corrosive gases. During the experiment, accelerated corrosion technology was used to improve the corrosion rate of the tower and grounding grid, and accelerated corrosion tests were conducted on building materials such as the tower and grounding grid.

## 2. Experimental setup

The selected experimental device structure includes a computer control unit, one-way valve, on-off valve, rotary flow meter, mass flow meter, electromagnetic valve, stainless steel cylinder, special gas cabinet, and test box. The experimental platform is shown in Figure 1.



Figure 1 Experimental platform

We select five common corrosive gases:  $\text{SO}_2$ ,  $\text{NO}_2$ ,  $\text{H}_2\text{S}$ ,  $\text{NH}_3$ , and  $\text{Cl}_2$ , with a 50-10000 ppm concentration range. The type of solution in the corrosion solution spray system is  $\text{NaCl}$  and  $(\text{NH}_4)_2\text{SO}_4$ . Its sedimentation is  $0.5\text{-}2 \text{ mL}/100 \text{ cm}^2\cdot\text{h}$ , and the concentration of salt solution is 8-20%. In temperature humidity alternating and constant temperature and humidity tests, the temperature range is  $5^\circ\text{C}\text{-}100^\circ\text{C}$ , and the humidity range is 15%~90%. We choose UVA or UVB for UV, and the two can be converted to each other. The process of simulating industrial pollution atmospheric environment cyclic accelerated corrosion test is shown in Figure 2. After the test is completed, the corrosion condition of the sample is studied. Firstly, the sample rust removal work begins. After the rust part is separated from the body, a brush is used to remove the rust part. After removing all the corroded parts, we remove the sample from the rust removal solution, clean it with distilled water and ethanol in sequence, dry it with a hair dryer, and place it in a dryer for 24 hours before weighing.

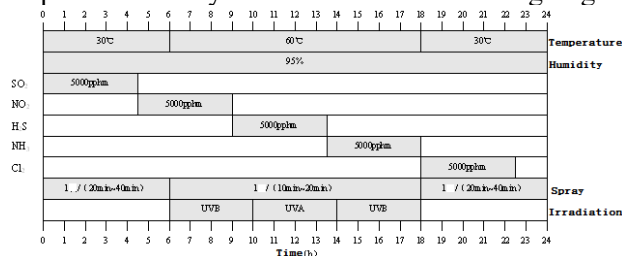


Figure 2 Flow chart of cyclic accelerated corrosion test for simulating industrial polluted atmospheric environment

## 3. Accelerated corrosion test

The commonly used galvanized steel material for the system was selected in the experiment, and the diameter of the designed material sample was  $\Phi 16 \text{ mm}$ , with a length of 5 cm, as shown in Figure 3. The two ends of the sample are sealed with epoxy resin and degreased with acetone.



Figure 3 Galvanized steel material for accelerated corrosion

Under different experimental conditions, the power supply is connected to a grounding material sample sealed at both ends. After the test, the sample is taken out, rust removed, cleaned, dried, and weighed to obtain the quality of the corroded sample. All results are calculated based on the mass loss per square decimeter per 24 hours, in  $\text{g}/\text{dm}^2\cdot\text{day}$ , using the following formula:

$$V_{\text{corr}} = \frac{24 \cdot \Delta m}{\Delta t \cdot A} \quad (1)$$

In the formula,  $V_{\text{corr}}$  is the corrosion rate,  $\text{g}/\text{dm}^2 \cdot \text{day}$ .  $\Delta m$  is the corrosion weight loss,  $\text{g}$ .  $\Delta t$  is the corrosion time,  $\text{h}$ .  $A$  is the exposed area of the sample,  $\text{dm}^2$ .

### 3.1 Effect of water content on corrosion of towers and grounding wires

Experimental conditions: The potential difference is maintained at DC 10 V, the area ratio of positive and negative electrodes is 70:1, the temperature is  $25^\circ\text{C}$ , and the accelerated corrosion time is 24 hours. The neutral soil moisture content used is 10%, 15%, 20%, 25%, and 30%. The water content and corrosion data are shown in Figure 4, and their relationship is shown in Figure 5. From Figure 4 and Figure 5, it can be seen that as the soil moisture content increases, the corrosion rate of the sample accelerates. The  $y=ax+b$  function fits the moisture content with the electrolytic accelerated corrosion rate. The exponential fitting function is  $y=3.1568x-0.2324$ , and the exponential fitting coefficient is  $R^2=0.9886$ . Therefore, the corrosion rate of the material is highly correlated with the soil moisture content.

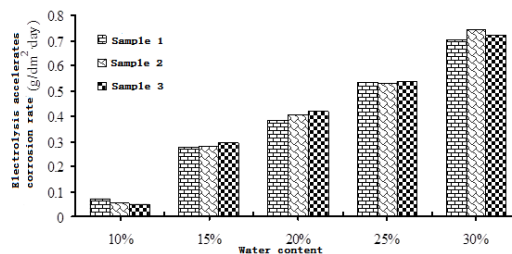


Figure 4 Accelerated corrosion rate data under different water content

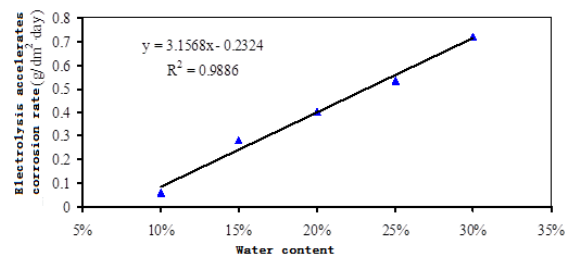


Figure 5 The relationship between water content and accelerated corrosion rate

### 3.2 Impact of temperature on corrosion of towers and grounding wires

Experimental conditions: The potential difference is DC 10 V, the area ratio of positive and negative electrodes is 70:1, the soil moisture content is 25%, and the accelerated corrosion time is 24 hours. The temperature choices are:  $15^\circ\text{C}$ ,  $20^\circ\text{C}$ ,  $25^\circ\text{C}$ ,  $30^\circ\text{C}$ , and  $35^\circ\text{C}$ . The accelerated corrosion data at different temperatures are shown in Figure 6, and the relationship between temperature and accelerated corrosion is shown in Figure 7. Figure 6 and Figure 7 show that as the experimental temperature increases, the corrosion rate of the sample becomes faster, and the coefficient of determination for exponential fitting is  $R^2=0.9862$ , which is highly correlated.

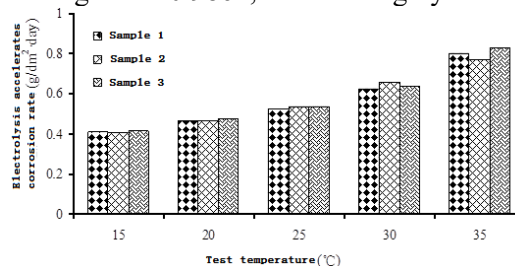


Figure 6 Accelerated corrosion data at different temperatures

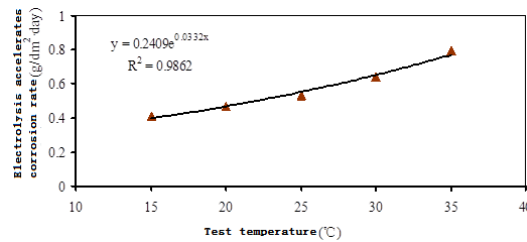


Figure 7 The relationship between temperature and accelerated corrosion

### 3.3 Effect of potential difference on corrosion of towers and grounding wires

Experimental conditions: The soil moisture content is 25%, the area ratio of anode and cathode is 70:1, the experimental temperature is 25°C, and the accelerated corrosion time is 24 hours. The potential difference in the sequence is 4 V, 6 V, 8 V, 10 V, and 12 V. The corrosion data under different cathodes' potential differences are shown in Figure 8, and the relationship between potential difference and accelerated corrosion is shown in Figure 9. From Figure 8 and Figure 9, it can be seen that as the potential difference increases, the accelerated corrosion rate increases linearly. The coefficient of determination for linear fitting  $R^2=0.973$  indicates a high linear correlation between potential difference and accelerated corrosion rate.

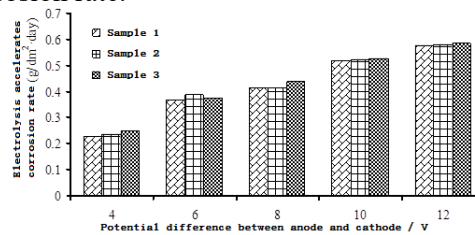


Figure 8 Accelerated corrosion data under different potential differences

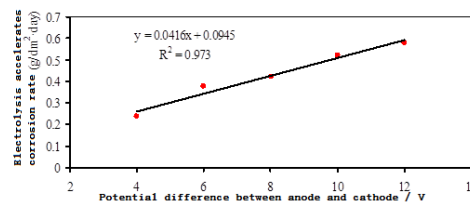


Figure 9 The relationship between potential difference and accelerated corrosion

### 3.4 Influence of area ratio of Yin and Yang Poles on corrosion of poles, towers, and grounding wires

Experimental conditions: The potential difference is DC 10 V, the soil moisture content is 25%, the temperature is 25°C, and the accelerated corrosion time is 24 hours. The areas of the Yin and Yang poles are 70:1, 90:1, 120:1, 180:1, and 360:1, respectively. The accelerated corrosion data under different area ratios of cathode and anode are shown in Figure 10, and the relationship between the area ratio of cathode and anode and accelerated corrosion is shown in Figure 11. Figure 10 and Figure 11 shows that as the area ratio of the cathode and anode increases, the accelerated corrosion rate increases in a logarithmic relationship. The determination coefficient  $R^2=0.9976$  using logarithmic fitting is highly correlated.

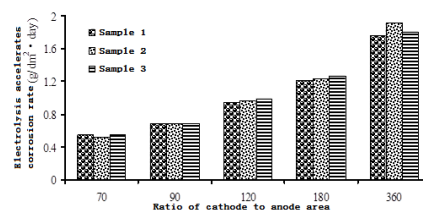


Figure 10 Accelerated corrosion data under the different ratios of the cathode to anode area

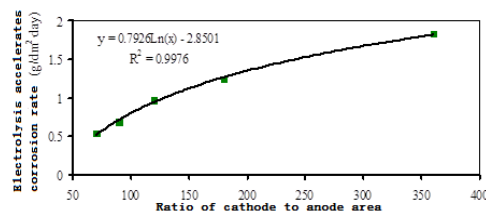


Figure 11 The relationship between the area ratio of cathode and anode and accelerated corrosion

#### 4. Multi-factor coupled orthogonal comprehensive experiments

To analyze the corrosion development characteristics of towers and grounding grids under multiple factors, six soil conditions were designed to determine the corrosion rate of materials, as shown in Table 1.

Table 1 Orthogonal test adopts the natural corrosion rate of galvanized steel in 6 soils

Number	1	2	3	4	5	6
Corrosion rate (g/dm <sup>2</sup> ·year)	0.5795	0.8751	1.5849	2.0916	2.5523	3.3342

Table 2 Factors and levels in accelerated corrosion orthogonal test

Factor	Parameter ①	Parameter ②	Parameter ③	Parameter ④
Test temperature	15°C	25°C	30°C	35°C
Water content	15%	20%	25%	30%
The potential difference between anode and cathode	6 V	8 V	10 V	12 V
The ratio of the cathode to anode area	70:1	90:1	120:1	180:1

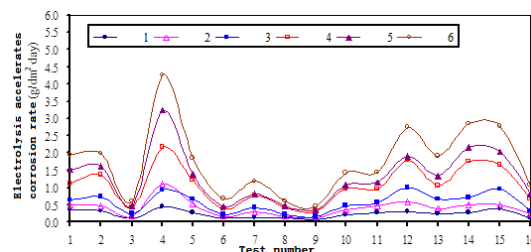


Figure 12 Accelerated corrosion multi-factor orthogonal test results

Based on different corrosion factors, experiments were designed under different accelerated corrosion factors and their parameters, as shown in Table 2. Through orthogonal comprehensive experiments, in Table 2, 16 tests are required for each soil type under different accelerated corrosion factors and parameters. The test results are shown in Figure 12.

Figure 12 shows that the factors affecting the accelerated corrosion rate in Soils 1, 3, and 4 are water content > area ratio of positive and negative electrodes > temperature > potential difference. In Soil 2 and Soil 6, it shows the area ratio of positive and negative electrodes > water content > temperature > potential difference. In Soil 5, it shows the area ratio of positive and negative electrodes > temperature > water content > potential difference. Therefore, the role of accelerating corrosion factors and soil with different corrosion rates is different, while the effect of potential difference is the smallest.

#### 5. Conclusion

This article first conducted a single-factor experiment and combined it with a single-factor analysis of variance to identify the factors that significantly impact the corrosion test results in the artificially accelerated corrosion test. Then, a multi-factor coupling experiment was conducted. The conclusions of this study are as follows:

(1) The single-factor test results of accelerated corrosion show that water content, the potential difference between positive and negative electrodes, the area ratio of positive and negative electrodes, and test temperature significantly impact the accelerated corrosion rate test results. In contrast, the effect of accelerated corrosion time on accelerated corrosion rate is not significant.

(2) Multiple factors influence the tower and grounding grid, and the accelerated corrosion factors and soil with different corrosion rates have different effects, while the potential difference plays the smallest role.

## References

- [1] Falk, Fuente D, Castano JG, Morcillo M. Long-term atmospheric corrosion of zinc [J]. *Corrosion Science*, 2007, 49: 1420-1436.
- [2] Jin Lei, Han W, Wang ZY, et al. Evolution of initial atmospheric corrosion of carbon steel in an industrial atmosphere [J]. *Journal of Materials Engineering and Performance*, 2016, 25: 5382-5390.
- [3] Lyon, Svensson JE, Johansson LG. The influence of CO<sub>2</sub> and NaCl on the atmospheric corrosion of zinc—a laboratory study [J]. *Journal of the Electrochemical Society*, 1998, 145: 2993-2999.
- [4] Drazic, Lillard S, Dragan P, et al. Isolated VS Interconnected Wind Turbine Grounding Systems; Effect on the Harmonic Grounding Impedance, Ground Potential Rise and Step Voltage [J]. *Electric Power Systems Research*, 2019, 34(20): 1530-1539.
- [5] Weihua Zheng, Xiaoyu Sun, Youping Fan. Study on electrochemical corrosion mechanism of steel foot of insulators for HVDC lines [J]. *IOP Conference Series: Materials Science and Engineering*, 2017, 242(1): 1605-1611.
- [6] Isshikawa T, Takeuchi K, Kandori K, et al. Transformation of  $\gamma$ -FeOOH to  $\alpha$ -FeOOH in acidic solutions containing metal ions [J]. *Colloids and Surfaces A: Physicochemical and Engineering Aspects*, 2005, 266(1-3): 155-159.
- [7] Wang J H, Wei F I, Shi H C. Modeling of atmospheric corrosion behavior of weathering steel in sulfur dioxide-polluted atmospheres [J]. *Corrosion*, 1996, 52(12): 900-909.
- [8] Weissenrieder J, Kleber C, Schreiner M, et al. In situ studies of sulfate nest formation on iron [J]. *Journal of the Electrochemical Society*, 2004, 151(9): B497-B504.
- [9] Arroyave C, Lopez F A, Morcillo M. The early atmospheric corrosion stages of carbon steel in acidic fogs [J]. *Corrosion Science*, 1995, 37(11): 1751-1761.
- [10] Johnson J B, Elliott P, Winterbottom M A, et al. Short-term atmospheric corrosion of mild steel at two weather and pollution monitored sites [J]. *Corrosion Science*, 1977, 17(8): 691-700.